DOI: 10.2298/CSIS120126052S

Application of Grid-based K-means Clustering Algorithm for Optimal Image Processing

Tingna Shi[a], Jeenshing Wang[b], Penglong Wang[a], and Shihong Yue[a]*

[a] School of Electrical Engineering and Automation, Tianjin University, Tianjin, China
[b] Department of Electrical Engineering, National Cheng Kung University, Tainan 701, Taiwan
Email: Shyue1999@tju.edu.cn (* Correspondence Author)

Abstract. The effectiveness of K-means clustering algorithm for image segmentation has been proven in many studies, but is limited in the following problems: 1) the determination of a proper number of clusters. If the number of clusters is determined incorrectly, a good-quality segmented image cannot be guaranteed; 2) the poor typicality of clustering prototypes; and 3) the determination of an optimal number of pixels. The number of pixels plays an important role in any image processing, but so far there is no general and efficient method to determine the optimal number of pixels. In this paper, a grid-based K-means algorithm is proposed for image segmentation. The advantages of the proposed algorithm over the existing K-means algorithm have been validated by some benchmark datasets. In addition, we further analyze the basic characteristics of the algorithm and propose a general index based on maximizing grey differences between investigated objective grays and background grays. Without any additional condition, the proposed index is robust in identifying an optimal number of pixels. Our experiments have validated the effectiveness of the proposed index by the image results that are consistent with the visual perception of the datasets.

Keywords: electrical tomography; number of pixels; image ronconstruction.

1. Introduction

Image processing plays an important role in a variety of applications such as robot vision, object recognition, and medical imaging [1][2][3]. Image segmentation is naturally a clustering course on the basis of pixels such as grey, veins, color and so on. As a result, the clustering analysis is widely applied in image segmentation.

With the rapid development of fundamental studies, more stringent demands are brought out for image segmentation. Under these circumstances, process tomography (PT) finds its unique role in studying the

multiphase flow phenomena encountered in chemical engineering fields, involving a number of tomographic techniques, such as X-ray, γ-ray, optical, ultrasonic, electrical, and nuclear magnetic resonance imaging. Among X-ray computed tomography (XCT) and electrical tomography (ET), an important issue of resolution in the XCT imaging process is to determine a proper number of pixels. Zhao *et al*. [4] proposed a multi-parameter method (includes area error and image centre position error) for the electrical capacitance tomography image evaluation. Graham and Adler [5], [6] defined the resolution in terms of fuzzy radius, and adopted the ratio between the radius of the interested region and that of the imaging region, the axial error and the image energy to evaluate the quality of reconstructed images. To date, however, none of the existing methods provides a universally acceptable solution to the number of pixels in any reconstructed x-ray images. In fact, these existing methods have many limitations. First, the methods to determine the number of pixels are often subjective with little satisfaction. Second, the objects under evaluation are binary images or gray-scale images. Third, some prior information such as image error resolution and duty ratio are considered in the evaluation process. The last but not the least, the evaluation process itself is not objective enough. For example, a known mesh of pixels is used during the whole image reconstruction process.

On the other hand, the K-means is one of the most frequently used methods for image segmentation [7] and its success chiefly attributes to the introduction of the belongingness of each image pixels. However, there are some key issues unsolved when using K-means clustering algorithm to deal with image segmentation, such as the determination of the number of clusters in a data set, the precise position of the cluster prototype, the real-time performance and initialization problem related to local optimization. Some research studies have attempted to overcome the above problems [8], [9]. Recently, an efficient grid-based k-means (G-K-means) algorithm for clustering has been proposed [10]. The G-K-means algorithm can efficiently overcome the above problems and take advantage over the existing K-means algorithms. In this paper, we further analyze the basic characteristics of the G-K-means algorithm, and demonstrate its advantages over the traditional K-means algorithm in image segmentation. Finally, we apply the G-K-means algorithm to image reconstruction in the x-ray field.

In this paper we propose a robust index to determine an optimal number of pixels based on maximizing grey differences between investigated grays and background objective grays. Results obtained by the finite element method (FEM) and Gent 4$^{@}$ software are also given. These experiments are conducted to validate the effectiveness and robustness of the proposed index.

2. Related work

In the following we present the main steps of both the K-means algorithm and

the G-K-means algorithm in terms of their iterative process and major problems in applications.

2.1. K-means algorithms

Let $X=\{x_i \mid i=1, 2, \ldots, n\}$ be a dataset with n data distributed in c clusters. The objective function of the K-means algorithm can be stated as

$$\min \ \sum_{i=1}^{K}\sum_{j=1}^{n} u_{ij} d_{ij}, \ s.t. \sum_{i=1}^{K} u_{ij} = 1, \qquad (1)$$

where $d_{ij} = ||x_j - v_i||$, v_i is the prototype of the i-th cluster, u_{ij} is the membership degree of the j-th data object to the i-th cluster, taken as either 0 or 1. In terms of the Lagrange optimization method, the optimal prototypes for Eq.(1) are

$$v_i = \sum_{j=1}^{n} u_{ij}^m x_j \Big/ \sum_{j=1}^{n} u_{ij}^m . \ , i=1, 2, \ldots, c \qquad (2)$$

Depending on the group of prototypes, the K-means algorithm assigns each object to the most similarity cluster based on the similar measure;

The above process is repeated and the algorithm stops if a convergence criterion is met. For the K-means algorithm, all membership degrees are expressed in a $n \times c$ matrix $U=[u_{ij}]$.

Although the K-means algorithm has been succeeded in many applications, it suffers largely from the following problems. First, the clustering results of the K-means algorithm greatly depend on its initialization, and are prone to fall into a local solution without a good initialization partition. Second, since the data assigning problem in the K-means algorithm is not optimal, and thus they are not suitable for applications where the membership degrees are assumed to represent typicality/compatibility with an elastic constraint, or are applied in noise circumstances. Third, the number of clusters must be known in advance when the FCM algorithm is used for clustering a dataset. In the past decades, many studies have been presented to overcome these problems, but these algorithms are little satisfied in image segmentation application except the G-K-MEANS algorithm as introduced below.

2.2. G-K-means algorithms

The G-K-means algorithm firstly divides the minimum closed set containing the data into optimal grid structures according to the optimal partition index [8], and then divides the grid structures into the online grid (to participate in the current iteration) and the offline grid (not to participate in the current iteration) as follows.

Definition 1. Mean center and geometric center. The mean center of a cluster is the arithmetic average of all object vectors in the cluster, while the geometric center of a cluster is the center of a minimal hypersphere that encloses all objects in this cluster.

Usually, the geometric center and the mean center of any cluster are different but are very close to each other if the cluster is symmetric (e.g. sphere(ellipsoid)-shaped).

Definition 2. On line grid and off line grid. Let *J* be an integer and *S* be a set of grids. A grid is called an online grid if the grid is one of top *K* high-density grids in *S*. Any grid that is not an online grid in *S* is called an offline grid.

All *J* grids in S are assigned into two sets $X_1 = \{G_1, G_2, ..G_K\}$ and $X_2 = \{G_{K+1}, G_{K+2}, ..., G_J\}$ such that

$$|G_{K+1}| \geq |G_{K+2}| \geq ,..., \geq |G_J| \ . \quad (3)$$

Thus X_1 is the set of online grids and X_2 is the set of offline grids.

Next, the steps which are similar to the K-means algorithm but have different mechanisms are carried out with the following objective function:

$$\text{Max} \sum_{i=1}^{K} | G_i - G_1 - G_2 - ... - G_{i-1} | / V_i \quad . \quad (4)$$

The G-K-means algorithm can work without the number of clusters *K* but with a database containing *n* objects based on the following six steps:

1. Choose *K* geometric centers of online grids as the initial mean centers, $v_1, v_2, \ldots, v_K$;
2. Repeat;
3. (Re)assign objects to G_i that is centralized on v_i, for $i = 1, 2, \ldots, K$;
4. Update cluster centers by

$$v_i = \sum_{j=1}^{|G_i|} u_{ij} x_j / u_{ij}, i = 1,2,...,K \quad (5)$$

5. Go to step 6 if a convergence criterion is met; Otherwise, go to Step 2.

Stop if there are no overlapping grids in X_1; Otherwise, add the offline grid with the highest density into X_1; go to Step 2.

The G-K-means algorithm can work under two states. If the number of clusters is known a priori, the value of *K* remains invariant in each iteration. Otherwise, Step 6 can automatically determine the final number of clusters. As opposed to the *K*-means algorithm, the G-K-means algorithm tends to find cluster centers in high-density areas while *K*-means cannot guarantee this point. Therefore, the cluster quality should be better from the viewpoint of density. Moreover, the algorithm assigns objects to grids, which needs much less computation than that of the Euclidean distance widely applied in many algorithms such as the *K*-means algorithm.

3. Basic characteristics of the G-K-means algorithm and optimal number of pixels

In the following, we first explore two key problems using the G-K-means algorithm in applications in terms of their basic characteristics and convergence domains. Then an index to determine an optimal number of pixels is proposed in image segmentation and X-ray image processing.

3.1. Basic characteristics and convergence of the G-K-means algorithm

◆ Objective function: The objective functions from the K-means to the G-K-means algorithm satisfy

$$\begin{matrix} \sum_{i=1}^{K}\sum_{j=1}^{n} u_{ij}d_{ij} \to min & \mapsto \\ \sum_{i=1}^{K} | G_i - G_1 - G_2 - ... - G_{i-1} | / V_i \end{matrix} \quad (6)$$

In (6), the objective function of the *K*-means algorithm is reformulated by a grid-based form in the G-K-means algorithm. Consequently, the maximum of the objective function in the *K*-means algorithm is attained by maximizing the average density of a group of online grids, G_i, i = 1, 2 , …, K. Thus the objective function in the *K*-means algorithm is data-object-based while the one in the G-K-MEANS algorithm is grid-based.

◆ Object assigning principle: Let each cluster be enclosed by a separate minimal hypersphere. When an object falls in a hypersphere, the object usually is closer to the geometric center of the hypersphere than any other geometric centers. In the *K*-means algorithm, the object is assigned to the cluster based on the hyperspheres. Consequently, the object assigning principle is to iteratively find *K* minimal hyperspheres that enclose *K* clusters respectively such that the geometric centers of these hyperspheres can be well-determined (see Fig.1).

Contrarily, the G-K-means algorithm iteratively applies *K* online grids that are centralized on v_1, v_2, …, v_K in place of *K* hyperspheres to enclose those objects in each clusters. Namely, an object is assigned to the *i*-th cluster if the object uniquely falls into the grid G_i that stands for the cluster, for i = 1, …, K. Finally, the G-K-means algorithm assigns all remaining objects that are not covered in any grid to their closest centers.

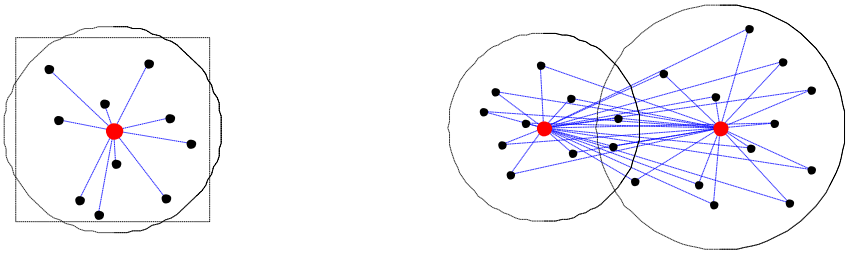

(a) (b)

Fig. 1. Comparison of the assigning principle of the *K*-means and the G-K-MEANS algorithms. (a) Grid-shaped and sphere-shaped neighborhoods; (b) All Euclidean distances in two partially overlapped clusters.

◆ Center update*:* Any new mean center in the G-K-means algorithm is locally computed by these objects limited to the related grid. In contrast, any mean center in the *K*-means algorithm may be affected by any object no matter how far it is from its involved center. In the G-K-means algorithm, if the distance between two mean centers of any two online grids is less than a threshold ε, the two online grids is considered as the same cluster. The low-populated one in the two online grids is removed from X_1 and the most high-populated offline grid in X_2 is added into X_1 in the next iteration. All iterations are terminated if the difference of the objective function values between two consecutive iterations is smaller than the threshold ε and $|X_1|=K$. Fig. 2 shows the flowchart of the G-K-means algorithm.

Comparing the convergence of the G-K-means algorithm with that of the K-means algorithm, we explain the problem as follows. The local convergence is an indicator which measures the risk for algorithms falling into a local minimum but it is difficult to theoretically analyze its characteristics. For the G-K-means algorithm and the K-means algorithm, the definitions of convergence are as follows.

Definition 3. Convergence domain. Choose a group of points as the initial clustering prototypes of the G-K-means or the K-means algorithms. Starting from the group of points, if the G-K-means algorithm or the K-means algorithm can converge to a local optimum, the group of points is called the convergence points of the algorithm. The set of all convergence points is called a convergence domain for the corresponding algorithm.

For example, we introduce a set of two-dimensional data points distributed in six irregular clusters data set to illustrate the concept of convergence domain, and to directly analyze the convergence of the experimental results. All data points are enclosed by a minimal closed set in which any point serves as a candidate of a convergence point to examine. The two algorithms group all data points over the minimum closed set which contains the space that minimizes the objective function. Denote $O_{\max}$ as a sufficiently small number (say 10^{-5}). For any group of initial points, if the difference between the final iteration is less than $O_{\max}$, we denote these data as convergence points. The set of all the convergence points consists of a convergence domain. Fig.

2 (b) and (c) show that the convergence of the G-K-means algorithm covers almost all the high-density areas (the yellow areas), only a small part of the high-density areas is uncovered, which is due to the impact of other clusters. It has no effect on the clustering results because the small part of the high-density online gray area is affected by adjacent clusters. Thus, they deviate from the high-density areas and become offline grids. Fig. 2 (a) clearly shows that the convergence domain of the K-means algorithm is less than that of G-K- means. This means that it is greater risk for the former than the latter to minimize the objective function. In particular, once the iteration point falling out of the domain of convergence there exists at least one cluster that is incorrectly distinguished because of lacking a flexible mediation mechanism between online and offline grids (pixels).

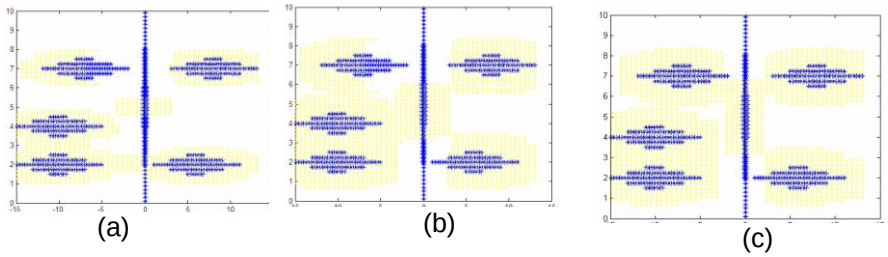

Fig.2. The convergence domain of different algorithms. (a) The convergence domain of K-means algorithm (b) The convergence domain of the G-K-MEANS algorithm with 16 initial grids. (c) The convergence domain of the G-K-MEANS algorithm with 32 initial grids.

3.2. X-ray imaging principle

The principle of the radiation attenuation is the first foundation of XCT. Assuming that the X-rays are monoenergetic from a parallel beam, the residual intensity of X-rays is attenuated by the materials that the X-rays pass through:

$$I = I_0 e^{\int_L \mu_m dl} \tag{7}$$

where μ_m is the mass attenuation coefficient *(*m^2/kg*)* mainly due to the photoelectric, Compton and pair production effects; and *dl* represents infinitesimal thin layer of the object (m). The corresponding expression of the projection data is

$$b_L = \ln(\frac{I_0}{I}) = \int_L \mu_m \rho ds \tag{8}$$

where ρ is the density of the object (kg/m^3). The image reconstruction techniques use the measured projection data as the *input* to calculate the

density distribution of the desired cross-section of the investigated sample as the *output*. Accordingly, the 2D image of the desired cross-section can be obtained. The mostly applied reconstruction techniques are divided into two categories, the back-projection reconstruction and the iterative reconstruction. As an example of the back-projection reconstruction technique, the filtered back-projection (FBP) technique is used in most commercial medical scanners and has proved to be extremely accurate and amenable to fast implementation. This technique can give a rather straightforward intuitive rationale because each projection represents a nearly independent measurement of the object.

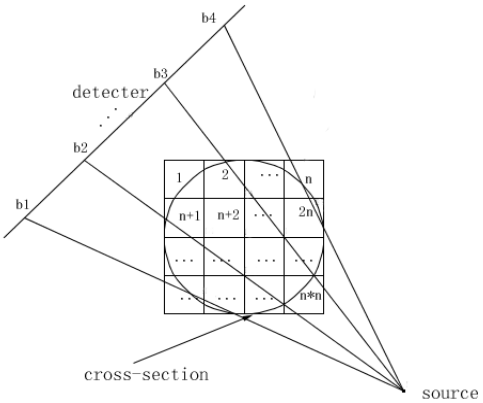

Fig.3. Illustration of the principle of XCT

As shown in Fig. 3, a 2D object is placed between the X-ray source and the detector. The investigated area is discretized by rectangular girds or triangular ones. The mathematical expression of the tomographic problem is given by the equations:

$$b = AX \text{ , i.e., } b_k = \sum_{j=1}^{M \times N} a_{kj}, k = 1,2,\ldots,K \quad (\mathbf{9})$$

where K is the total number of the projections, $M \times N$ is the total number of pixels across the area, a_{kj} means the weighting factor for the contribution of pixel j to the projection element b_k. The goal is to determine the unknown image X when the experimental projections b are available. The weighting factor, a_{kj} , is calculated based on the geometrical consideration as the intersection length/area of the kth projection ray with the image pixel j. In the discrete form, the aim of image reconstruction for the X-ray field is to find the unknown X from the known b by using Eq. (10), that is

$$X = A^{-1}b \quad (\mathbf{10})$$

However, the direct analytical solution for Eq. (9) does not exist since the inverse problem is both nonlinear and ill-posed, little noise in the measured data could cause large errors in the estimated conductivity. Consequently, it is necessary to use numerical techniques to approximate S^{-1} as accurate as

possible after applying some residual criterion. One efficient criteria is minimal least error defined as

$$||b - AX||_2^2 \to \min \tag{11}$$

Eq. (11) is used to identify the optimal values of *X*. Many variants of Eq. (11) have proposed to solve the ill-posed problem among which the most used ET image reconstruction algorithms are the linear back projection (LBP). In the LBP algorithm the conductivity distributions are assumed to comprise a number of discrete regions within the measurement space such that the conductivity within each region is constant. According to Eq. (10),

$$X = A^T B / A^T u_\lambda, \quad s.t.\ u_\lambda = [1,1,\ldots,1] \tag{22}$$

Eq. (12) shows that the grey values of any pixels are calculated using a weighted form in the algorithm [13].

In this paper, we first use the LBP algorithm for X-ray imaging reconstruction to examine the optimality of space resolutions of X-ray imaging under various numbers of pixels. Different from the existing LBP algorithm, these calculated values by Eq. (12) are indirectly applied to reconstruct any images. Inversely, we denote $\overline{X}$ as the set of all values of X from Eq. (12) and then the G-K-means algorithm is applied to cluster all members in $\overline{X}$. Finally, these members in different clusters are endowed to different gray while the members in the same cluster have the same gray. These gray degrees over all pixels thus reflect the information of the spatial distributions of the investigated materials.

When applying the existing K-means clustering algorithm, one needs to predefine the number of clusters *K*. Currently, there are two applicable ways to determine the number of clusters. First, in some cases, there is a priori knowledge of the actual number of clusters since the multiphase flows in a measured field consists of determined components such that these multiphase flows consist of as the gas, water, and oil in a crude oil transmission pipe. Thus we take the number of clusters that is larger than three since the X-ray imaging inevitably contains the trail traces that have to be represented by some additional clusters of more than three. Second, if there is no prior number of clusters available, the issue of determining the number of clusters falls into the category of clustering validity indices in a given dataset [14], i.e., the number of clusters can be determined by a proper function called the clustering validity index [15], [16]. There are some efficient validity indices in fuzzy clustering such as the partition entropy (PE) proposed by Bezdek [17], the Xie-He index [18], etc. As the running time increases, these indices work well for some datasets. However, these methods to determine the number of clusters have their limitations. Essentially, most of them are specifically designed to the K-means-like algorithm. As compared, the G-K-means algorithm can automatically suggest an optimal number of clusters and overcome most limitations of the existing K-means clustering algorithm in image segmentations.

An optimal index to determine the optimal number of pixels

The optimal number of pixels plays an important role in image processing. When applying the G-K-means algorithm, the number of pixels is determined by the grid size; that is, the grid size can affect the partitions of the G-K-means algorithm. An overlarge grid may contain two or more clusters while too small grid may lead to too many online grids to be assigned to the same cluster and a significant increase of CPU possessing runtime. Basically, a cluster consists of the centric high-density grids while the surrounding low-density grids and empty grids separate the given data structure into different groups (clusters) that aggregates similar data objects (see Fig. 4). All nonempty grids are ordered into three sets of grids: $D(t)$, t = 1, 2, 3, satisfying that the object number of any grid in $D(t)$ is larger than any other grid in $D(t+1, j)$, t = 1, 2. The two classes of high and low populated grids respectively cover the center and margin areas of all clusters. The larger differences between the two classes of grids are, the easier identification of different clusters by a clustering algorithm is. This is the core idea hidden in (10). It has been demonstrated that there must be an optimal value of the ration between $D(1)$ and $D(3)$ for any dataset with any cluster structure, and the optimal value indicates that most of the clusters in the dataset have been broken by the partitioned grids [9]. Consequently, the ration can act as the upper bound of initial number of grids and predict the optimal grid size.

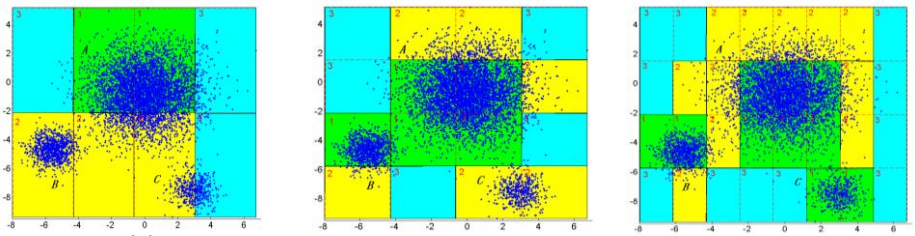

Fig.4. Three classes of grids under different grid sizes in $D(1)$, $D(2)$ and $D(3)$ from high to low density correspond to center, inner, and margin areas of most clusters in a dataset with three clusters. (a)–(c) corresponds to three classes of grids, respectively. The same color indicates the same class of grids

Accordingly, if the number of pixels can be incorrectly determined, a good-quality segmented image cannot be guaranteed. We thus propose a general index based on maximizing grey differences between investigated objectives and background as follows.

Consider a pixel dataset $M = [x_1, x_2, ..., x_n] \in R^{d \times n}$, where each column of M, $x_i = (x_{i1}, x_{i2}, ..., x_{id})^T \in R^d$, is a singleton data object in a d-dimensional data space. For example, when the number of ray resources is 16, d=16. Let $\varepsilon_{\max}$ and $\varepsilon_{\min}$ be the maximal and minimal distances between any pair of data objects in M respectively and $\varepsilon \in [\varepsilon_{\min}, \varepsilon_{\max}]$. We take a number of equidistant breaking points $\varepsilon_1, \varepsilon_2, ..., \varepsilon_{s-1}, \varepsilon_s$ from ε_1 to ε_s to partition ε,

$\varepsilon_1 = \varepsilon_{\min}$, $\varepsilon_s = \varepsilon_{\max}$, where s is the number of breaking points. A breaking point s_k can be characterized as

$$\varepsilon_k = \varepsilon_1 + (k-1)\Delta,\ k = 1,2,\ldots,s \tag{33}$$

where Δ is the distance between any two adjacent breaking points. Let $N_{\varepsilon_k}(x_j)$ be the subset of the data objects in the ε_k -neighborhood of x_j, $k = 1,2,\ldots,s$; $j = 1,2,\ldots,n$. Group all subsets of x_j into three sets of grids: $D(s,\ \varepsilon_k)$, s = 1, 2, 3, such that the density of any subset in $D(t,\ \varepsilon_k)$ is greater than any other subset in $D(t+1,\ \varepsilon_k)$, t = 1, 2. Hereafter, $|\bullet|$ denotes the number of data objects in the contained set. The optimal neighborhood size, say GPI, is determined by maximizing the ratio of $|D(1,\ \varepsilon_k)|$ and $|D(3,\ \varepsilon_k)|$; that is,

$$\text{GPI} = \arg\max_{\varepsilon_k} \{|D(1,\ \varepsilon_k)| \,/\, |D(3,\ \varepsilon_k)|\}, \tag{44}$$

Hereafter GPI is called a general partitioning index (GPI) in this paper. The two classes of subsets in $D(1,\ \varepsilon_k)$ and $D(3,\ \varepsilon_k)$ correspond to the centric and margin locations of all clusters. If $\varepsilon \to \varepsilon_{\min}$ each data point will have no neighborhood and $\varepsilon_{OPT} = 1$ while $\varepsilon \to \varepsilon_{\max}$, the space will degenerate to a subset. The differences between any pair of subsets will disappear and $\varepsilon_{OPT} = 1$. Consequently, there must be at least one maximum on Eq. (8) without any additional conditions. In the experiments, we will graphically show these maximums.

GPI in (9) aims at maximizing grey differences between investigated objectives and background since the investigated objectives respond to these pixels whose components have larger values while the background responds to these pixels whose components have smaller values.

Fig.5 shows the flowchart of our proposed approach in image segmentation application.

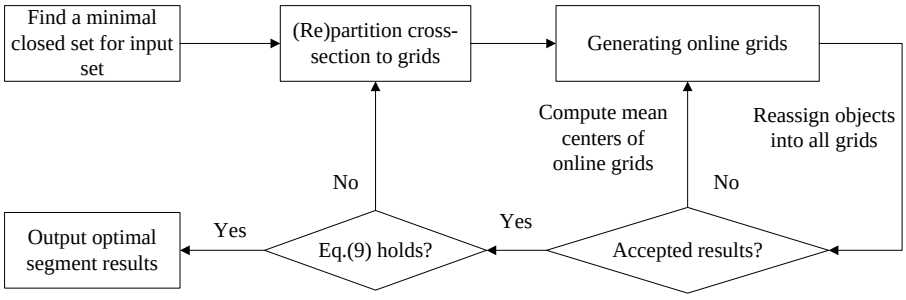

Fig.5. Flowchart of the proposed approach in image segmentation application.

4. Experiments

In this section we conduct two groups of experiments to validate of the effectiveness of the G-K-means algorithm and GPI respectively. In addition, we apply the K-means algorithm to the experiments under various numbers of pixels using the same datasets. These experiments are performed in the X-ray sensitiveness fields and analyzed by space resolution. Here the space resolution refers to the relative error of all *n* pixels in a partitioned image as

$$\zeta = \frac{1}{n}\sum_{j=1}^{n}\frac{(g_j - g_j^*)}{g_j^*} \tag{55}$$

where g_j is the reference grey degree of the *j*-th pixel, that is the real grey value; g_j^* is the grey value of the *j*-th pixel in the reconstructed image, *j*=1, 2,…, *n*; and ξ is the average of all errors of K pixels.

4.1. Image segmentation in a group of benchmark datasets

We apply the color and grey templates of the well-known Lena image as original images, and use the K-means and G-K-means algorithms for image segmentation. For the original Lena color images, the information is kept into $m \times n \times 3$ data matrix. We give each element in term of the array of pixel values as red(G) blue(B), green(G). Assuming the matrix I stored the information of Lena color pixel, we can get the color value of each pixel, denoted as $I_R = I(:,:,1)$, $I_G = I(:,:,2)$, $I_B = I(:,:,3)$. A three-dimensional matrix are firstly constructed by I_R, I_G and I_B, and then we make use of the above two algorithm for image segmentation. The segmentation quality is measured by the following two indices:

1)The mis-segmented number of pixels. It is an important index to evaluate the segmented images in practice and is further formulated as Eq. (15).

2) Time cost. The runtime of an algorithm decides its applicable range. In case of most situations with the real-time demands, the K-means algorithm is too slow to be applied.

Fig. 5 and Fig. 6 visually show the segmented images by the above two algorithms. These results of the two algorithms are obtained under two conditions: (1) the number of clusters is selected from 2 to 12, and the best segmented image is shown in Figs. 5(b) and 5(c), and Figs. 6(b) and 6(c) respectively. (2) Four times of initializations are implemented in order to overcome the local minimum when we apply the K-means algorithm. In contrast to the two original images in Fig. 6 and Fig. 7, the segmented images from the G-K-means algorithm are clearer and tidier than those from the K-means algorithm, and more close to the real templates. Table 2 further verifies that the two statistical indices of the G-K-means algorithm are

superior to those of the K-means algorithm. In particular, the G-K-MEANS algorithm is rather stable and robust, and hardly is affected by the initialization problems that often are encountered in the applications of the K-means algorithm.

(a) (b) (c)

Fig.6. Segmented results of standard Lena image. (a) Original Lena image template. (b) K-means. (c) G-K-means.

(a) (b) (c)

Fig.7. Segmented results of standard Lena image by the two algorithms. (a) Lena image template. (b) K-means (c) G-K-means.

Table 1. Comparison of the image segmentation quality by two algorithms.

Algorithms	Mis-segmented pixel number	Relative error	Runtime (Seconds)
K-MEANS	1177	0.2619	0.2349
G-K-means	1026	0.1914	0.0143

4.2. Image segmentation in X-ray fields

The datasets of this set of simulations are obtained from Geant4 [19]. The tested original images are five and twenty-five circles with continuously distributed materials, as shown in Table 3(a) and Table 4(a).

These circles have the same material component and thus should be shown as the same gray degree. The background must respond to two kinds of different grey degrees since there is a class of trail traces at least. We perform the LBP algorithm with various numbers of pixels (e.g., grids in the FEM) for image reconstruction, while the values of GPI are computed to find

its maximum for the optimal number of pixels. For comparison, the space resolutions of Eq. (10) are computed. As the number of pixels gradually decreases, these images of different space resolutions are obtained. It can be observed that GPI can clearly attain their maximums and, at the same time, the space resolution of the images that respond to the maximum by Eq. (10) attains its maximum. Please note that Eq. (10) is a subjective evaluation of space resolution due to dependence of necessary reference image. Inversely, GPI works well without any other information except the reconstructed image itself. Consequently, GPI perfectly is an objective evaluation index. After calculating these values of Eq. (7) for all pixels, we apply the G-K-MEANS algorithm to cluster all members in the set of the obtained values. When GPI attains its maximum, the corresponding number of pixels is optimal. In fact, the trail traces in a reconstructed image of the maximum of GPI is minimal, and the boundary of investigated objectives (see Table 3 (f) and Table 4 (d)). It can visually be observed that the trail traces in other images, whose values of GPI are far away from the maximum, are widely distributed, and even some circles are incorrectly connected to the same area or some circles cannot be found. Thus, these images show that GPI can better distinguish the optimal X-ray images by the determination of the optimal number of pixels. Table 3 gives the quantitative description of the imaging results of these two algorithms. Table 3 shows that all the space resolutions of the G-K-MEANS algorithm by Eq. (10) are superior to those of the K-means algorithm, while the time cost is far less that of the K-means algorithm.

Fig. 8 summarizes the curve of GPI values in the above two groups of X-ray images. It can be seen from Fig. 3 that the two maximums are dominantly larger than other values. Thus GPI can clearly predict the optimal number of pixels and evaluate the X-ray image of the best space resolution. GPI can represent different physical meanings and can work objectively without any additional information. Specifically, to measure the robustness of GPI, the radiuses of these images in the two sets are taken by a group of very different values. Fig. 7 shows that the maximums of GPI are encountered in most radiuses. This demonstrates GPI is useful and efficient in most datasets. Indeed, in some datasets, GPI is inefficient and thus there still is a necessity to improve its performance.

Table 2. Original and reconstructed images that correspond to the original image of five circles.

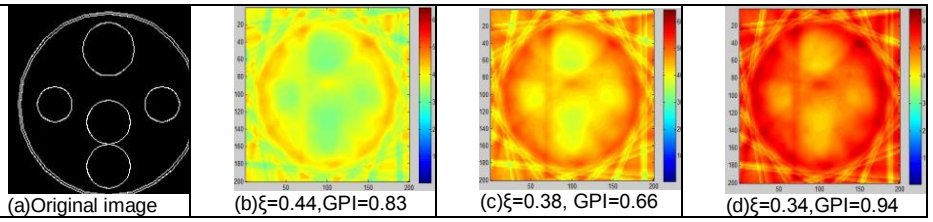

(a)Original image (b)ξ=0.44,GPI=0.83 (c)ξ=0.38, GPI=0.66 (d)ξ=0.34,GPI=0.94

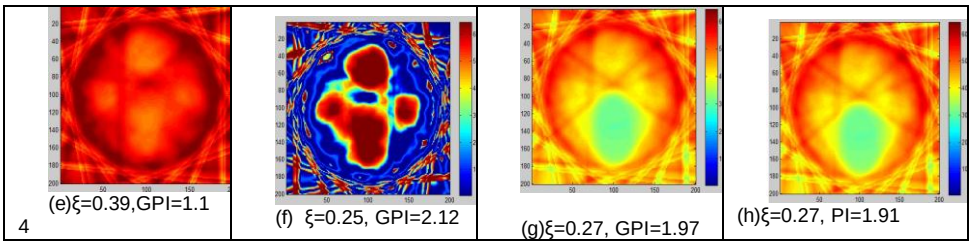

Table.3. Original and reconstructed images that correspond to the original image of twenty-five circles.

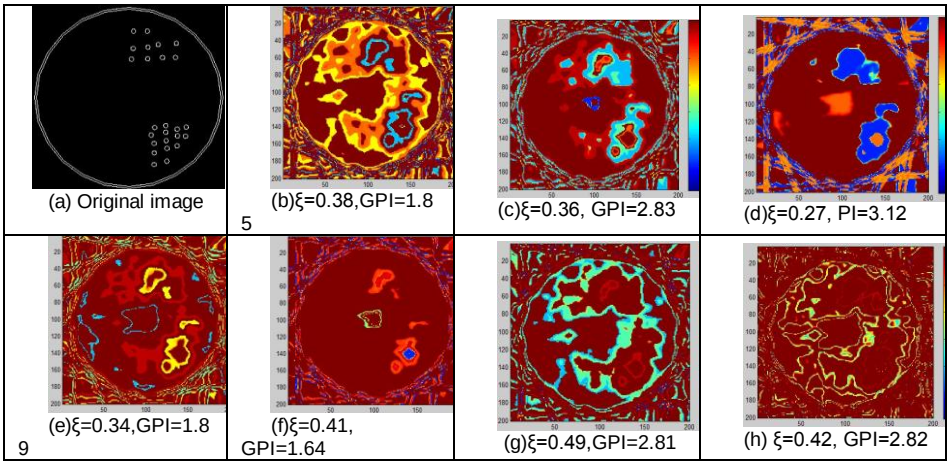

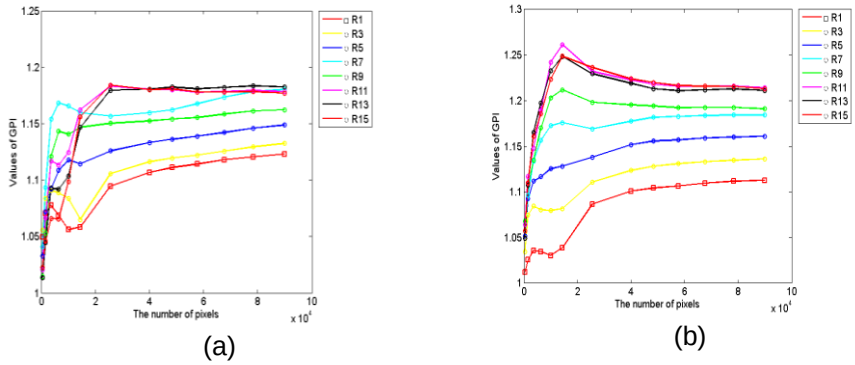

Fig. 8. Maximums of GPI in reconstructed images under different numbers of pixels from the LBP algorithms. (a) and (b) correspond to the two sets of three and twenty-five circles, respectively. The signs "R×" stand for a group of various radii.

Table.4. Comparison of the image segmentation quality by two algorithms

Algorithms	Mis-segmented pixel number	Relative error	Runtime (Seconds)
K-MEANS	2387	0.3697	0.2590
G-K-MEANS	2011	0.2273	0.0875

5. Conclusion

Image segmentation is the foundation of image analysis, image understanding and pattern recognition. However, due to the lack of fundamental measures to deal with the problem of image segmentation, the current common clustering algorithms cannot achieve unsupervised clustering. In this paper we apply the G-K-means algorithm to image segmentation applications. The G-K-means algorithm has not only linearly computational complexity but also simple and effective operation. The advantage of the G-K-means algorithm over the existing K-means algorithm has been demonstrated by its fast convergence and clustering performance. Our experimental results have validated that the proposed index for determining the optimal number of pixels is effective and comprehensible in its reconstructed images of high spatial resolution.

Acknowledgment. This work is supported by the National Science Foundation of China under Grant No. 61774014, 60572065, 60772080 and the National Science Foundation of Tianjin under Grant N0.08JCYBJC13800.

References

1. Zhang Y.: Image segmentation. Beijing: Science Press. (2001).
2. Olson C. F.: Maximum-Likelihood Image Matching, IEEE Trans. Patt. Anal. Mach. Intell., vol. 24, no. 6, pp. 853-891. (2002)
3. Pham D.L.: Partial models for fuzzy clustering, Computer Vision and Image Understanding, vol.84, pp.285-297. (2001)
4. Dudukovic, M.P.: Opaque multiphase flows: experiments and modeling. Experimental Thermal and Fluid Science, vol. 26, no.3, pp. 747-753. (2002)
5. Ahmed M. N., Yamany S M, and Mohamed N.: A modified fuzzy C-means algorithm for bias field estimation and segmentation of MRI data, IEEE Trans. Medical Imaging, vol.21, no.3, pp.193~199. (2002)
6. Banholzer, W.F., Spiro, C.L., Kosky, P.G., Maylotte, D.H.: Direct imaging of time-averaged flow patterns in a fluidized reactor using X-ray computed tomography. Industrial & Engineering Chemistry Research 26, 763-770. (1987)
7. Bartholomew, R.N., Casagrande, R.M.: Measuring solids concentration in fluidized systems by Gamma-ray absorption. Industrial & Engineering Chemistry, vol.49, pp.428-436. (1957)
8. Zhao J, Fu W and Hu Q.: Investigation of evaluating method for reconstructed

image quality of electrical capacitance tomography system. Journal of Guangxi University (Science), Vol. 28, pp. 61-64 (2003)
9. Dyakowski T., Edwards, R.B., Xie, C. G. Williams, R.A.: Application of capacitance tomography to gas solid flows. Chemical Engineering Science , vol.52, pp.2099-2112. (1997)
10. Grassler, T., Wirth, K.E.: X-ray computer tomography—potential and limitation for the measurement of local solids distribution in circulating fluidized beds. Chemical Engineering Journal, vol. 77, pp.65-73. (2000)
11. Harvel G.D., Hori, K., Kawanishi, K., Chang, J. S.: Real-time crosssectional averaged void fraction measurements in vertical annulus gas liquid two-phase flow by neutron radiography and X-ray tomography techniques. Nuclear Instruments and Methods in Physics Research Section A, vol.371, no.3, pp.544-554. (1996)
12. Harvel, G.D., Hori, K., Kawanishi, K., Chang, J.S.: Cross-sectional void fraction distribution measurements in a vertical annulus two-phase flow by high speed X-ray computed tomography and real-time neutron radiography techniques. Flow Measurement and Instrumentation, vol. 10, no.4, pp.259-266. (1999)
13. Xie X.L., Beni G.: A validity measure for fuzzy clustering, IEEE Trans. Pattern Anal. Mach. Intell., vol.13, no.8, pp. 841–847, 1991.
14. Yue S., Wang J., Gao T., Wang H.: An unsupervised grid-based approach for clustering analysis, Science China-Information Science. vol.53, no.6, pp. 1372-1384. (2010)
15. Yue S., Wei M., Wang J., Wang H.: A general grid-clustering approach, Patt. Recognition Letter, vol.29, no.9, pp.1372-1384. (2008)
16. Kai, T., Misawa, M., Takahashi, T., Tiseanu, I., Ichikawa, N., Takada, N.: Application of fast X-ray CT scanner to visualization of bubbles in fluidized bed. Journal of Chemical Engineering of Japan, vol.33, no.6, pp.906-911. (2000)
17. Kantzas, A., Kalogeraki, N.: Monitoring the fluidization characteristics of polyolefin resins using X-ray computer assisted tomography scanning. Chemical Engineering Science 51 (10). (1979)
18. Kantzas, A., Wright, I., Kalogerakis, N.: Quantification of channeling in polyethylene resin fluid beds using X-ray computer assisted tomography (CAT). Chemical Engineering Science, vol. 52, no.13, pp.2023-2033. (1997) Http://geant4.slac.stanford.edu/installation/

Tingna Shi received the B.Sc. and M.S. degrees in the Electrical engineering department from Zhjiang University in China, respectively. In 2009 she received the Ph.D degree in the School of electrical engineering and automation from Tianjin University in China. And she works in the School of electrical engineering and automation from Tianjin University as an associate professor from 2003 to 2012 and a professor now. Her research interests include wind power, electrical technique, and intelligence control.

Penglong Wang received the B.Sc. degree in the Automation department from Tianjin University of Technology in China. From 2011 till now he studies as a student for the M.S. degree in the Tianjin University in China. His research interests include pattern recognition, information fusion and intelligence control.

Jeenshing Wang received the B.S and M.S. degrees in electrical engineering from the University of Missouri, Columbia, in 1996 and 1997, respectively, and the Ph.D. degree from Purdue University, West Lafayette, IN, in 2001. He is currently an Associate Professor with the Department of Electrical Engineering, National Cheng Kung University, Tainan, Taiwan. His research interests include computational intelligence, intelligent control, clustering analysis, and optimization.

Shihong Yue received the B.Sc. degree in the mathematics department from Yili Normal University, Xinjiang in China. And the M.S. and Ph.D degree in application mathematics from the Xi`An University of Technology and in the mathematics department from Xi`An Jiaotong University, in 1997 and 2000, respectively. From 2000 till 2004, he works in Institute of Industrial process control from Zhejiang University as a postdoctoral and received deputy professor in July 2001. As a visiting professor, he works in the department of computer science and Information engineering, Taiwan, in 2002. From 2004 till now, he works as a professor in the School of Electrical Engineering and Automation from Tinjin University. His research interests include pattern recognition, information fusion and intelligence control.

Received: January 26, 2012; Accepted: November 17, 2012.